Available online at www.sciencedirect.com
SCIENCE DIRECT
Earth and Planetary Science Letters 248 (2006) 244–252
EPSL
www.elsevier.com/locate/epsl

Assessing the likelihood of volcanic eruption through analysis of volcanotectonic earthquake fault–plane solutions

D.C. Roman [a,*,1], J. Neuberg [a], R.R. Luckett [b]

[a] School of Earth and Environment, University of Leeds, Leeds LS2 9JT, United Kingdom
[b] British Geological Survey, Murchison House, Edinburgh, United Kingdom

Received 6 October 2005; received in revised form 22 May 2006; accepted 22 May 2006
Available online 7 July 2006
Editor: S. King

Abstract

Episodes of volcanic unrest do not always lead to an eruption. Many of the commonly monitored signals of volcanic unrest, including surface deformation and increased degassing, can reflect perturbations to a deeper magma storage system, and may persist for years without accompanying eruptive activity. Signals of volcanic unrest can also persist following the end of an eruption. Furthermore, the most reliable eruption precursor, the occurrence of low-frequency seismicity, appears to reflect very shallow processes and typically precedes eruptions by only hours to days. Thus, the identification of measurable and unambiguous indicators that are sensitive to changes in the mid-level conduit system during an intermediate stage of magma ascent is of critical importance to the field of volcano monitoring. Here, using data from the ongoing eruption of the Soufrière Hills Volcano, Montserrat, we show that ~90° changes in the orientation of double-couple fault–plane solutions for high-frequency 'volcanotectonic' (VT) earthquakes reflect pressurization of the mid-level conduit system prior to eruption and may precede the onset of eruptive episodes by weeks to months. Our results demonstrate that, once the characteristic stress field response to magma ascent at a given volcano is established, a relatively simple analysis of VT fault–plane solutions may be used to make intermediate-term assessments of the likelihood of future eruptive activity.

Keywords: volcanic hazards; volcano monitoring; fault–plane solutions; volcanotectonic earthquakes; Soufrière Hills Volcano

1. Introduction

The Soufrière Hills Volcano, Montserrat, began to erupt in July 1995, and lava extrusion continues at present. This eruption has been monitored comprehensively from the beginning, and many aspects have been described extensively [1]. The eruption stopped in March 1998, but high-frequency, or 'volcanotectonic' (VT; [2]), earthquake swarms, SO_2 output, and phreatic explosions continued at high levels for another year and a half [3,4] (e.g., Fig. 1b), raising questions during this period as to whether the eruption would restart in the near future [4]. The eruption restarted in November 1999, heralded only by a sharp increase in the number of low-frequency (hybrid and long-period [2]) earthquakes days to weeks before fresh lava reached the surface (Fig.

* Corresponding author. Tel.: +1 813 974 2838; fax: +1 813 974 2654.
E-mail address: droman@cas.usf.edu (D.C. Roman).
[1] Present address: Department of Geology, University of South Florida, 4202 E. Fowler Avenue, SCA 528, Tampa, FL 33620, USA.

0012-821X/$ - see front matter © 2006 Elsevier B.V. All rights reserved.
doi:10.1016/j.epsl.2006.05.029

1a). Dome-building then continued for four more years. The eruption stopped again in August 2003. For the next two years, surface deformation, SO_2 degassing, and shallow explosions continued, again prompting questions about the likelihood of future eruptive activity, until the eruption restarted in August 2005.

Our goal in this study was to determine whether analysis of fault–plane solutions for VT earthquakes recorded at Soufrière Hills could be used to detect the arrival of ascending magma in the mid-level conduit system, thus providing a relatively early warning of an impending eruption. Systematic changes in the orientation of fault–plane solutions for VT earthquakes have been observed at a number of active volcanoes [5,6] and have been linked to dilation of the magmatic conduit system [7], and the quality of the VT data recorded at Soufrière Hills combined with the episodic nature of this eruption makes it an ideal case for assessing the usefulness of this phenomenon as a forecasting tool.

2. Methods and data analysis

We produced a large catalog of high-quality fault–plane solutions that spanned nine years and several phases of the eruption, using simple techniques that realistically could be used in near-real time, especially during a crisis situation, and then analyzed this catalog to determine whether a temporal correlation exists between eruptive activity and fault–plane solution orientation. We relocated all VT earthquakes recorded on the Montserrat Volcano Observatory (MVO) digital seismic network from its inception in October 1996 through July 2005, using the program Hypocenter [8] and a standard 1D velocity model [9]. Locations of the MVO digital seismic stations and of VT earthquakes recorded by the MVO digital network during our study period are shown in Fig. 2. The MVO digital seismic network has been comprised of a mixture of seven to eight Guralp CMG-40T broadband three-component seismometers and Integra LA100 1 Hz vertical seismometers. Seismic

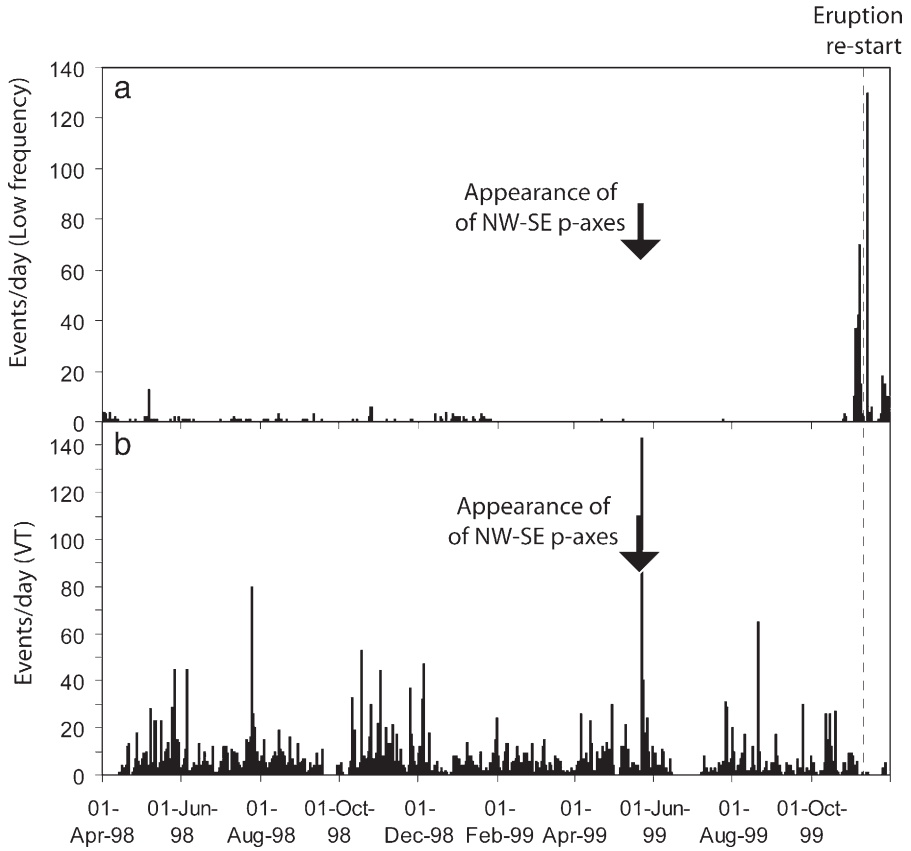

Fig. 1. Number of events per day recorded by the MVO digital seismic network during a pause in eruption at Soufrière Hills in 1998–1999: (a) the number of low-frequency (hybrid/long-period) events per day; (b) the number of VT earthquakes per day. The approximate timing of the eruption restart is indicated by the gray dashed line. Black arrows show the timing of a ~90° change in the orientation of fault–plane solution *p*-axes.

data are digitized at 75 Hz sampling and then telemetered to the MVO where they are recorded in both event-detected and continuous mode. Additional details on the stations and data acquisition systems are given by Neuberg et al. [10]. For all earthquakes for which we produced a high-quality (horizontal and vertical location errors <1.5 km, azimuthal gap <180°, RMS <0.20) hypocenter location, we attempted to calculate a double-couple fault–plane solution based on first-motion polarities using the program FPFIT [11]. The resulting fault–plane solutions were evaluated for quality and rejected if they did not meet all of the following criteria (e.g. [12,13]): at least six clear first-motion polarities, unique or similar multiple solutions, misfit of less than 15% (no more than one discrepant first motion), STDR (station distribution ratio, a measure of data distribution around the hypocenter) ≥ 0.40, uncertainty in strike, dip, and rake of ≤ 25°, and pressure (*p*-) and tension (*t*-) axis regions that cover ≤ 25% of the focal sphere. Waveform recordings of teleseisms were used to identify stations with reversed polarities during the study period, and all identified polarity reversals were accounted for during calculation of fault–plane solutions. Fault–plane solutions for VT earthquakes occurring in the seismogenic volume below the Soufrière Hills vent are found to be insignificantly affected by small changes in raypaths induced by different velocity models (B. Baptie, personal communication), or by the inclusion of S/P

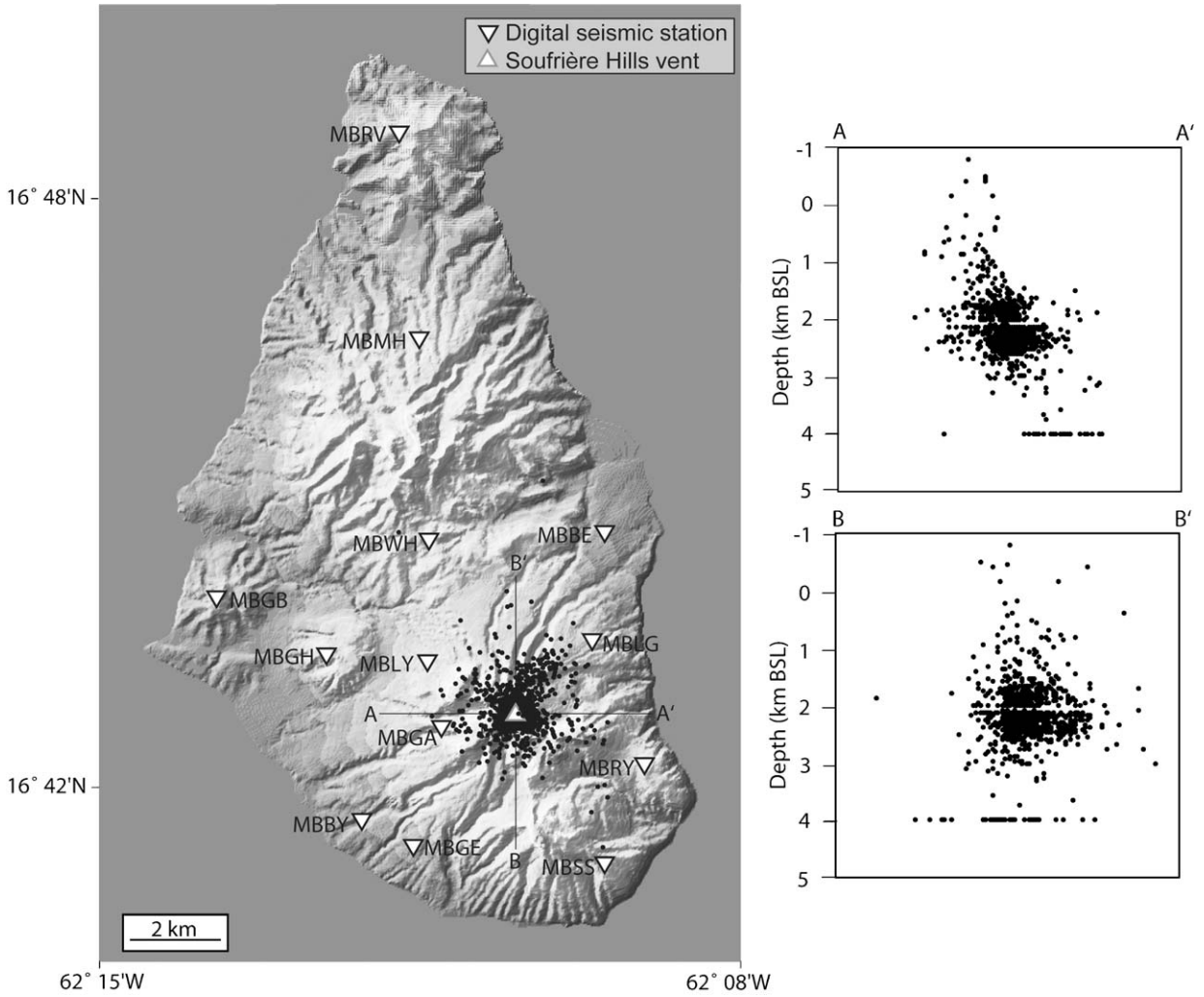

Fig. 2. Map showing names and locations of all digital seismic stations operated on Montserrat, as well as the approximate location of the Soufrière Hills vent, and all well-constrained VT epicenters from October 1996 to July 2005 (black dots). N–S and E–W cross sections of hypocenter locations are also shown. Please note that the digital seismic network consisted of a subset of all stations shown, typically 7–8 of the stations at a given time.

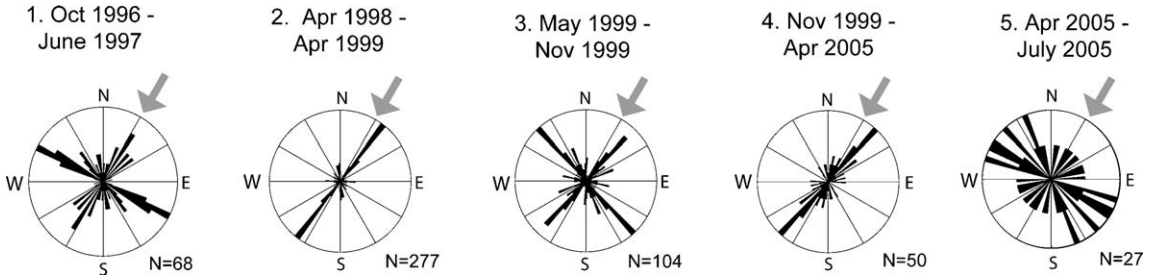

Fig. 3. Qualitative analysis of double-couple fault–plane solutions for VT earthquakes recorded at Soufrière Hills. Rose diagrams 1 to 5 show the azimuths of *p*-axis orientations in five different periods of the eruption. *N* indicates the number of fault–plane solutions in each Rose diagram. Gray arrows indicate the azimuth of inferred regional maximum compression. Only fault–plane solutions with *p*-axis dip $<60°$ are considered in this and in subsequent analyses.

amplitude ratios in addition to first-motion polarity data. Out of 5319 VT earthquakes recorded during the study period, we were able to produce 1235 high-quality hypocentral locations and 551 well-constrained double-couple fault–plane solutions. Earthquakes with well-constrained fault–plane solutions range in magnitude from 1.5 to 3.9 M_L. Almost all of the VT seismicity during our study period was located within a roughly cylindrical volume with a radius of <1 km and depth range of 1–3 km BSL, centered beneath the eruptive vent (Fig. 2). 95% of the high-quality fault–plane solutions show pure or oblique strike-slip mechanisms (*p*-axis dip $<60°$).

A qualitative inspection of the individual fault–plane solutions indicates a clear and obvious change in the dominant *p*-axis orientation (taken here as a proxy for the orientation of maximum compressive stress; see Appendix A) with time through our study period (Fig. 3). Specifically, a large number of fault–plane solutions with *p*-axes oriented approximately NW–SE (perpendicular to a constant NE–SW-oriented *p*-axis trend) occur during three time-spans: October 1996–June 1997, May 1999–November 1999, and April–July 2005 (Periods 1, 3, and 5 in Fig. 3). During the other two periods, April 1998–May 1999 and November 1999–April 2005 (Periods 2 and 4 in Fig. 3), most fault–plane solutions *p*-axes are oriented approximately NE–SW. The period from July 1997 to March 1998 is not considered because damage from pyroclastic flows made the seismic network unsuitable for calculating fault–plane solutions during this time. Based on the orientation of eroded dikes on neighboring islands [14,15] and on fault–plane solutions for large regional earthquakes, the orientation of regional maximum compressive stress around Montserrat appears to be arc-normal or NNE–SSW to NE–SW; thus the episodic NW–SE trend in fault–plane solution *p*-axis orientation observed in Periods 1, 3, and 5 is approximately 90° to inferred regional maximum compression, consistent with a simple geometric relationship between the preferred orientation of a dike-like conduit in a deviatoric stress field (in this case NE–SW) and the orientation of maximum compressive stress in a localized stress field induced by the inflation of that conduit (in this case NW–SE) [7]. Thus we believe that the appearance of the NW–SE trend in *p*-axis orientation results from stresses induced by the inflation of a NE

Table 1
Number of data and averages of quality criteria for hypocenters and fault–plane solutions in each time period considered

Period	No. of FPS [a]	Total no. of located earthquakes	FPS hypos: horizontal error (km)	FPS hypos: vertical error (km)	FPS hypos: azimuthal gap (deg)	FPS hypos: RMS (s)	FPS: # of polarities	FPS: misfit (% of polarities)	STDR [b]	Strike uncertainty (deg)	Dip uncertainty (deg)	Rake uncertainty (deg)
1	68	145	0.8	1.0	105	0.11	6.8	9	0.63	10	9	14
2	277	636	1.0	1.0	138	0.08	6.5	2	0.68	13	17	18
3	104	253	0.8	0.9	102	0.07	6.8	3	0.68	12	15	18
4	50	131	0.8	0.9	114	0.09	7.1	2	0.65	12	15	17
5	27	69	0.9	0.8	107	0.08	6.4	0	0.60	9	10	10

[a] FPS: fault–plane solutions.
[b] STDR: station distribution ratio (a measure of data distribution around the hypocenter – a low STDR indicates that the polarities are generally close to calculated nodal planes).

trending dike or system of dikes beneath the vent. Descriptions of fault–plane solution data comprising each period are given in Table 1. We note that there is no relationship between the number of fault–plane solutions in a period and the presence or absence of NW–SE oriented *p*-axes, indicating that the appearance of the episodic *p*-axis trend is not an artifact of the amount of available data. We also note that there is no apparent spatial or depth dependence of *p*-axis orientation in our data set, although it is unclear whether this is due to the fact that the majority of the earthquakes for which we calculated fault–plane solutions occur within a small seismogenic volume with dimensions approximately equal to the horizontal and vertical location uncertainty of the hypocenter locations.

Our fault–plane solution data indicate that the conduit for the Soufrière Hills eruption is a dike or system of dikes trending NE–SW, approximately parallel to inferred regional maximum compression, which inflate in a NW–SE direction (perpendicular to regional maximum compression [16]). Additional supporting evidence for a NE–SW trending dike feeding the Soufrière Hills eruption is given by Aspinall et al. [9], who describe a large cluster of VT earthquakes occurring in August 1995 that is elongated in a NE–SW direction and located just NE of the summit vent. There is, however, some disagreement in the literature about the orientation of the Soufrière Hills conduit system. Mattioli et al. [17] model surface deformation recorded by a GPS network from October 1995 to July 1997 using

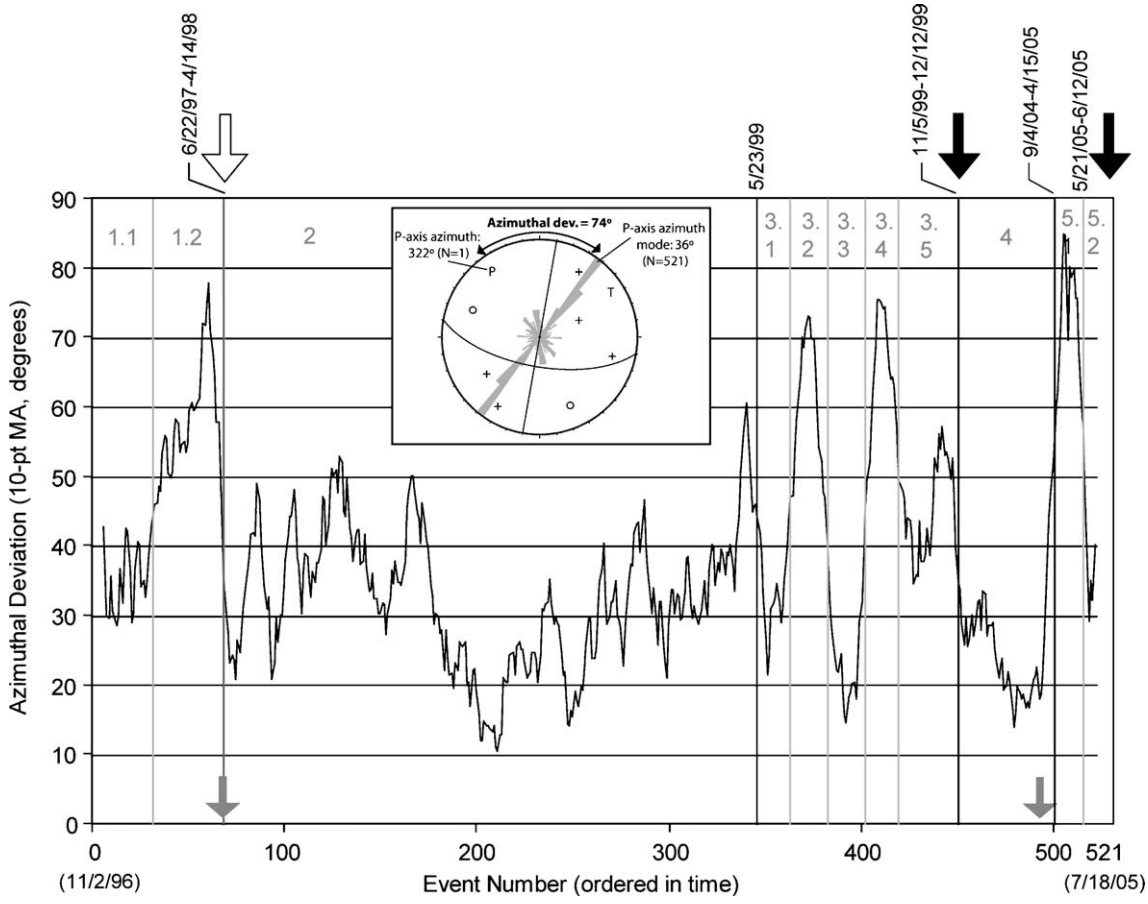

Fig. 4. Ten-point moving average of azimuthal deviation through time for the Soufrière Hills fault–plane solutions. Statistically significant (99% confidence) breaks in the curve are indicated as solid vertical lines (black lines indicate qualitatively identifiable changes as shown in Fig. 3; gray lines indicate additional changes identified through statistical analysis). The two eruption restarts are indicated by heavy black arrows at the top of the graph, and the start of Vulcanian sequence (effusive to explosive transition) is indicated by the white arrow at the top of the graph. Dates of the major breaks are indicated, as are major changes in the seismic network (change of at least two instruments, gray arrows at bottom of graph). Periods of uniform stress are numbered and correspond to numbered Rose diagrams in Figs. 3 and 5. Inset: Example of the measurement of 'azimuthal deviation', which is the difference in degrees between the azimuth of a single fault–plane solution *p*-axis and the azimuthal mode of all fault–plane solution *p*-axes in the analyzed data set (for our data set, 36°).

a combined deflating Mogi source and an inflating dike trending NW–SE (their best-fit dike source trends 140°). However, they only tested dikes with a narrow range of azimuths (130°–150°), and their best-fit combined source model, acknowledged to be non-unique, produces large misfits at two out of six GPS stations.

The observed changes in the dominant orientation of fault–plane solution *p*-axes through time have also been quantified and analyzed for statistical significance. For fault–plane solutions that are pure or oblique strike-slip, we define 'azimuthal deviation' as the difference between individual *p*-axis azimuths and the modal value for the entire data set (inset, Fig. 4). We plot a moving average of the azimuthal deviation vs. event number for all earthquakes ordered in time in Fig. 4, and analyze for all statistically significant changes in the curve, which indicate significant changes in the orientation of fault–plane solution *p*-axes [18,19].

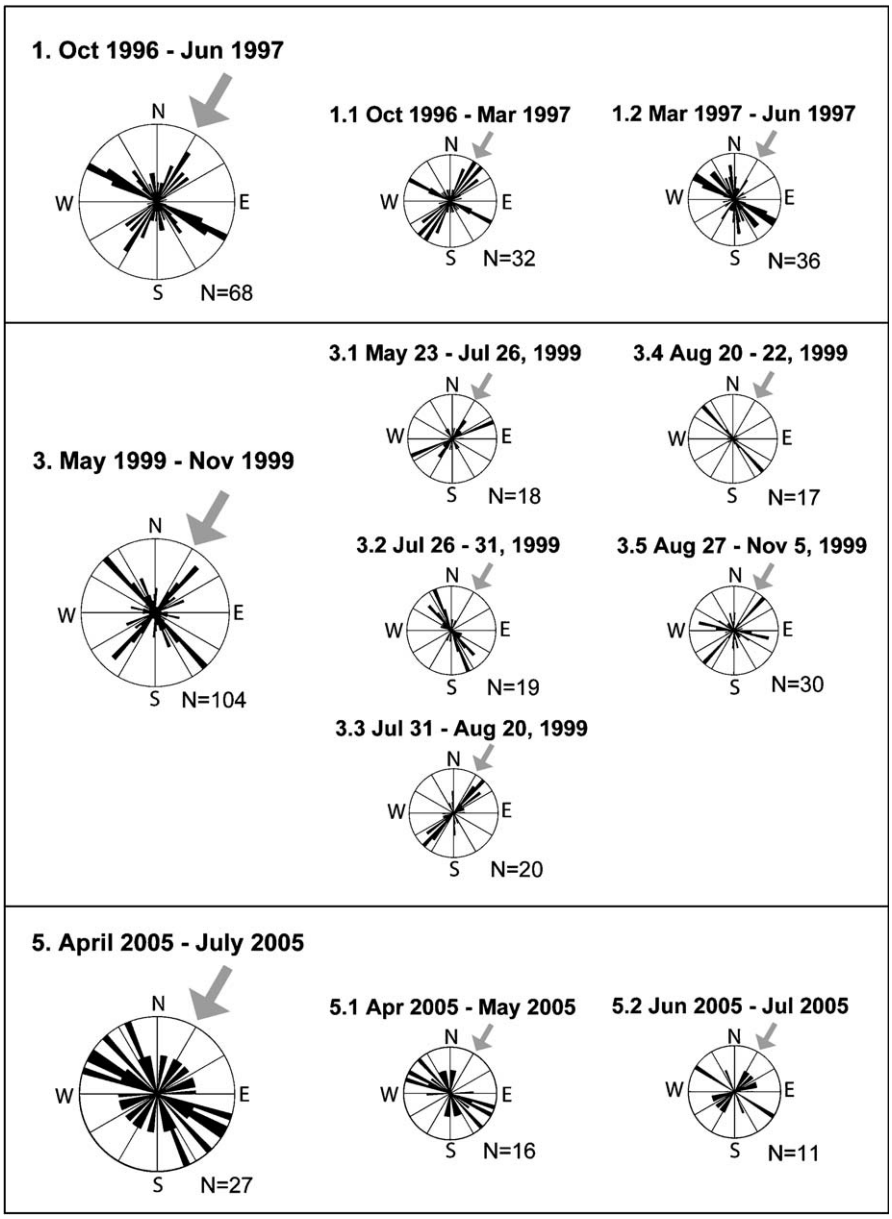

Fig. 5. Rose diagrams of the azimuths of *p*-axis orientations for statistically significant (at the 99% confidence level) subperiods of Periods 1, 3, and 5. Numbered subperiods correspond to those shown in Fig. 4. *N* indicates the number of fault–plane solutions in each Rose diagram. Gray arrows indicate the azimuth of inferred regional maximum compression.

Major changes in *p*-axis orientation (significant at the 99% confidence level) occur between the five periods identified qualitatively (Periods 1–5 in Figs. 3 and 4), as well as in March 1997 (during Period 1), four times during May–November 1999 (during Period 3), and between May and June 2005 (during Period 5). Rose diagrams of fault–plane solution *p*-axis orientation for subperiods in Periods 1, 3, and 5 are shown in Fig. 5. Since the determination of fault–plane solutions can be biased by a change in the configuration of the seismic network, we note that only one significant change in *p*-axis orientation corresponds to a major change in the configuration of the seismic network (in April 1998).

3. Discussion

It is clear that double-couple fault–plane solutions for VT earthquakes are sensitive to changes in the state of the Soufrière Hills volcanic system, as the three periods during which fault–plane solutions with NW–SE trending *p*-axes are observed precede changes in the state of the eruption. The first occurred during a period of magma extrusion immediately preceding a sequence of explosive Vulcanian eruptions that began in June 1997, the second occurred during the six months leading up to the restart of the eruption in November 1999, and the third occurred during the four months prior to the restart of the eruption in August 2005, coincident with a sequence of explosions, an increase in seismicity, and a change in the tilt signal from deflation to inflation that began in April 2005 [20]. Thus our results suggest that the occurrence of earthquakes with NW–SE trending *p*-axes at Soufrière Hills generally precedes the onset of eruptive activity by weeks to months, and may also indicate an impending transition from effusive to explosive activity during dome-building periods.

The occurrence of earthquakes with NW–SE trending *p*-axes beginning in May 1999 provides a compelling example of the usefulness of fault–plane solution analysis as a monitoring tool. Surface deformation and SO_2 emissions, signals that would typically intensify months prior to an eruption, remained elevated after the eruption ceased in March 1998, making them difficult to interpret in terms of the likelihood of future eruptive activity. It is possible that the continuously elevated levels of deformation and gas emissions during the 1998–1999 break in the eruption resulted from continued input of new magma into a chamber at approximately six km depth BSL [4], which was somehow prevented from migrating further up into the conduit system during the early part of this period. In addition, VT earthquake activity between 0 and 5 km BSL remained elevated following the March 1998 pause (Fig. 1b), adding more ambiguity to the situation. While the occurrence of VT earthquakes is often taken as an indicator of stresses transmitted into the wall rock by an influx of magma, VT earthquakes can also occur in response to depressurization and subsequent host-rock relaxation [21,22]. Based on our fault–plane solution data, conduit deflation and consequent relaxation of host rock appears to have been the cause of VTs recorded at Soufrière Hills from March 1998 to May 1999. Aside from a significant increase in the number of low-frequency earthquakes days to weeks prior to the restart of the eruption (Fig. 1a), the appearance of NW–SE trending *p*-axes in fault–plane solution data beginning in May 1999 was the only clear pre-eruption change in monitoring data identified to date, and thus would have provided a strong indication that the conduit system was undergoing a major repressurization months before magma reached the surface.

At Soufrière Hills, the occurrence of earthquakes with NW–SE trending *p*-axes may be either continuous or discontinuous from their first appearance to the onset of eruption, resulting in potential difficulties in interpreting data for eruption forecasting. For example, beginning in October 1996, earthquakes with NW–SE trending *p*-axes occurred frequently at Soufrière Hills and their rate of occurrence increased significantly as the period progressed (Figs. 4 and 5, Periods 1.1 and 1.2). In contrast, beginning in May 1999, earthquakes with NW–SE trending *p*-axes occurred intermittently over the six months leading up to the restart of the eruption (Figs. 4 and 5, Periods 3.1–3.5). Similarly, during the buildup to the renewal of eruptive activity in 2005, earthquakes with NW–SE trending *p*-axes were more frequent in the first two months of the four months of unrest preceding eruption (Figs. 4 and 5, Periods 5.1–5.2). In the first case, a forecast that eruptive activity would occur or increase in intensity made at the first observation of NW–SE trending *p*-axes would have been correct and consistently enforced by additional data collected throughout the period. In the second and third cases, however, a forecast of renewed eruptive activity made when the first earthquakes with NW–SE *p*-axes were observed would have ultimately been correct but possibly weakened throughout the period by the later disappearance and reappearance of the NW–SE *p*-axis trend. Based on the patterns we observe in the Soufrière Hills fault–plane solution data, it appears that while the occurrence of earthquakes with NW–SE oriented *p*-axes should be taken as an indication that the conduit system is inflating and thus an eruption is likely, the disappearance of these earthquakes does not necessarily indicate that an

eruption is unlikely to occur. There is no clear explanation for the variation in fault–plane solution orientation observed during Periods 3 and 5. It is possible that the discontinuous NW–SE *p*-axis trend during these periods reflects an unstable or uneven repressurization of the conduit during the buildup to eruption, or a lag between pressurization of the mid-level conduit and arrival of magma at the surface; however, additional data from Soufrière Hills or other volcanoes will be necessary to test this hypothesis.

Our results demonstrate that double-couple fault–plane solution analysis is an important tool for assessing the state of the Soufrière Hills Volcano. While this technique does not provide a basis for forecasting the exact timing of eruptive activity, it functions as a true forecasting tool for the likelihood of eruption, since this analysis is not dependant on knowledge of other variables that can only be determined in hindsight. There is strong evidence that volcanic fault–plane solution analysis may be an applicable monitoring technique at other restless or active volcanoes. Changes in fault–plane solution orientation similar to those observed at Soufrière Hills have been observed at a number of other volcanoes [5,6,23,24]. However, some eruptions clearly have not been accompanied by changes in the orientation of fault–plane solutions [24,25], so it may be necessary to establish the characteristic stress field response for a given volcano (either using data from a previous eruption or from a previous phase of an ongoing eruption) before this type of monitoring can be used confidently [26]. In many cases, it may be possible to begin the implementation of routine volcanic fault–plane solution analysis by making minor reconfigurations or upgrades to existing seismic monitoring networks and beginning to assess the background or normal orientation of fault–plane solutions through analysis of background VT seismicity. It may also be possible to integrate this technique with other forecasting techniques based on analysis of VT earthquakes (e.g. [27]) to form a more refined forecasting procedure that provides information on both the likelihood and the timing of an eruption. We strongly argue for continued testing and application of this relatively simple technique, which may be unique in its ability to provide a basis for formulating mid-range forecasts of the likelihood of volcanic activity from easily obtainable and routinely acquired data.

Acknowledgements

This work would not have been possible without the assistance of the current and former staff of the Montserrat Volcano Observatory, who collected, processed, and supplied the earthquake data and supplementary information necessary for the analyses. Special thanks are given to former MVO seismologists Art Jolly, Lars Ottemoller, and Brian Baptie for their assistance and input during the course of this study. We also wish to thank Willy Aspinall and David Green for their assistance, and Steve Sparks, Chris Kilburn, and an anonymous reviewer for constructive suggestions for improving the manuscript. This project was supported by a NERC postdoctoral fellowship to D.C. Roman.

Appendix A

In this study we take the fault–plane solution *p*-axis orientation as a proxy for the orientation of maximum compressive stress in the volume of rock hosting the earthquake. We are unable to invert groups of fault–plane solutions to obtain a formal stress tensor (e.g. [5,28]) because our fault–plane solution data clearly violate the primary assumption of most inversion methods (e.g. [29]) that the stress field in the inverted volume is homogeneous. Models of Coulomb stress changes induced by dike inflation demonstrate that the inflation-induced stress field will vary with position around the inflating dike (Fig. 1 of [7]); thus unless the size of the inflating dike is known to be significantly larger than the location uncertainty of VT earthquakes occurring in the immediate vicinity of the inflating dike, it is generally inadvisable to invert VT fault–plane solutions for formal stress tensors. The fault–plane solution *p*-axis orientation, which marks the position of the principal compressional axis of the moment tensor, may in reality differ significantly from the orientation of maximum compressive stress, depending on the orientation of pre-existing planes of weakness (faults) and on the value of internal friction [30]. Our solution to this inherent ambiguity is to examine large numbers of fault–plane solution *p*-axis orientations for a given period or volume plotted as Rose diagrams to highlight the major trends in *p*-axis orientation that most likely represent the actual orientations of maximum compressive stress present in the studied volume (e.g., Fig. 9 of [5]).

References

[1] T.H. Druitt, B.P. Kokelaar, The Eruption of Soufrière Hills Volcano, Montserrat, from 1995 to 1999, Geological Society, London, 2002, 664 pp.

[2] A.D. Miller, R.C. Stewart, R.A. White, R. Luckett, B.J. Baptie, W.P. Aspinall, J.L. Latchman, L.L. Lynch, B. Voight, Seismicity associated with dome growth and collapse at the Soufriere Hills Volcano, Montserrat, Geophys. Res. Lett. 25 (1998) 3401–3404.

[3] M. Edmonds, C. Oppenheimer, D.M. Pyle, R.A. Herd, G. Thompson, SO_2 emissions from Soufrière Hills Volcano and their relationship to conduit permeability, hydrothermal interaction and degassing regime, J. Volcanol. Geotherm. Res. 124 (2003) 23–43.

[4] G.E. Norton, R.A. Herd, R. Watts, W.P. Aspinall, S.R. Young, C. Bonadonna, B. Baptie, M. Edmonds, C.L. Harford, A.D. Jolly, S.C. Loughlin, R. Luckett, G. Mattioli, R.S.J. Sparks, Pyroclastic flow and explosive activity of the lava dome of Soufriere Hills Volcano, Montserrat, during a period of no magma extrusion (March 1998 to November 1999), in: T.H. Druitt, B.P. Kokelaar (Eds.), The Eruption of Soufrière Hills Volcano, Montserrat, from 1995 to 1999, Geological Society, London, 2002, pp. 467–481.

[5] D.C. Roman, S.C. Moran, J.A. Power, K.V. Cashman, Temporal and spatial variation of local stress fields before and after the 1992 eruptions of Crater Peak Vent, Mount Spurr Volcano, Alaska, Bull. Seismol. Soc. Am. 94 (2004) 2366–2379.

[6] K. Umakoshi, H. Shimizu, N. Matsuwo, Volcano-tectonic seismicity at Unzen Volcano, Japan, 1985–1999, J. Volcanol. Geotherm. Res. 112 (2001) 117–131.

[7] D.C. Roman, Numerical models of volcanotectonic earthquake triggering on non-ideally oriented faults, Geophys. Res. Lett. 32 (2005), doi:10.1029/2004GL021549.

[8] B.R.E. Lienert, J. Havskov, A computer program for locating earthquakes both locally and globally, Seismol. Res. Lett. 66 (1995) 26–36.

[9] W.P. Aspinall, A.D. Miller, L.L. Lynch, J.L. Latchman, R.C. Stewart, R.A. White, J.A. Power, Soufrière Hills eruption, Montserrat, 1995–1997: volcanic earthquake locations and fault–plane solutions, Geophys. Res. Lett. 25 (1998) 3397–3400.

[10] J. Neuberg, B. Baptie, R. Luckett, R. Stewart, Results from the broadband seismic network on Montserrat, Geophys. Res. Lett. 25 (1998) 3661–3664.

[11] P.A. Reasenberg, D. Oppenheimer, "FPFIT, FPPLOT, and FPPAGE: Fortran computer programs for calculating and displaying earthquake fault_plane solutions", U.S. Geol. Surv. Open_File Rep. 85-739, 1985.

[12] A.D. Jolly, R.A. Page, J.A. Power, Seismicity and stress in the vicinity of Mount Spurr Volcano, south central Alaska, J. Geophys. Res. 99 (1994) 15305–15318.

[13] E. Giampiccolo, C. Musumeci, S.D. Malone, S. Gresta, E. Privitera, Seismicity and stress-tensor inversion in the Central Washington Cascade Mountains, Bull. Seismol. Soc. Am. 89 (1999) 811–821.

[14] G. Wadge, J.B. Shepherd, Segmentation of the Lesser Antilles subduction zone, Earth Planet. Sci. Lett. 71 (1984) 297–304.

[15] G. Wadge, The dykes and structural setting of the volcanic front in the Lesser Antilles island arc, Bull. Volcanol. 48 (1986) 349–372.

[16] K. Nakamura, K.H. Jacob, J.N. Davies, Volcanoes as possible indicators of tectonic stress orientation: Aleutians and Alaska, Pure Appl. Geophys. 115 (1977) 87–112.

[17] G.S. Mattioli, T.H. Dixon, F. Farina, E.S. Howell, P.E. Jansma, A.L. Smith, GPS measurement of surface deformation around Soufriere Hills volcano, Montserrat from October 1995 to July 1996, Geophys. Res. Lett. 25 (1998) 3417–3420.

[18] Z. Lu, M. Wyss, Segmentation of the Aleutian plate boundary derived from stress direction estimates based on fault–plane solutions, J. Geophys. Res. 101 (1996) 803–816.

[19] M. Wyss, Z. Lu, Plate boundary segmentation by stress directions: Southern San Andreas Fault, California, Geophys. Res. Lett. 22 (1995) 547–550.

[20] V. Bass, S. Loughlin, R. Luckett, G. Ryan, M. Strutt, R. Syers, B. Baptie, V. Hards, A. O'Monghain, G. Norton, Volcanic activity at Soufrière Hills Volcano during a long period of decline, in: Soufriere Hills, Ten Years on Conference Proceedings, 2005.

[21] S.E. Barker, S.D. Malone, Magmatic system geometry at Mount St. Helens modeled from the stress field associated with posteruptive earthquakes, J. Geophys. Res. 96 (1991) 11883–11894.

[22] J. Mori, R.A. White, D.H. Harlow, P. Okubo, J.A. Power, R.P. Hoblitt, E.P. Laguerta, A. Lanuza, B.C. Bautista, Volcanic earthquakes following the 1991 climatic eruption of Mount Pinatubo: strong seismicity during a waning eruption, in: C.G. Newhall, R.S. Punongbayn (Eds.), Fire and Mud: Eruptions and Lahars of Mount Pinatubo, Philippines, Univ. Washington Press, Seattle, 1996, pp. 339–350.

[23] D. Patane, P. De Gori, C. Chiarabba, A. Bonaccorso, Magma ascent and the pressurization of Mount Etna's volcanic system, Science 299 (2003) 2061–2063.

[24] E. Fukuyama, A. Kubo, H. Kawai, K. Nonomura, Seismic remote monitoring of stress field, Earth Planets Space 53 (2001) 1021–1026.

[25] M. Ukuwa, H. Tsukahara, Earthquake swarms and dike intrusions off the east coast of Izu Peninsula, central Japan, Tectonophysics 253 (1996) 285–303.

[26] D.C. Roman, K.V. Cashman, The origin of volcanotectonic earthquake swarms, Geology 34 (2006) 457–460.

[27] C.R.J. Kilburn, Multiscale fracturing as a key to forecasting volcanic eruptions, J. Volcanol.Geotherm. Res. 125 (2004) 271–289.

[28] G. Barberi, O. Cocina, V. Maiolino, C. Musumeci, E. Privitera, Insight into Mt. Etna (Italy) kinematics during the 2002–2003 eruption as inferred from seismic stress and strain tensors, Geophys. Res. Lett. (2004), doi:10.1029/2004GL020918.

[29] J.W. Gephart, D.W. Forsyth, An improved method for determining the regional stress tensor using earthquake focal mechanism data: application to the San Fernando earthquake sequence, J. Geophys. Res. 89 (1984) 9305–9320.

[30] C.H. Scholz, The Mechanics of Earthquakes and Faulting, 2nd Edition, Cambridge University Press, 2002, 471 pp.